J. Mech. Phys. Solids 156 (2021) 104604

Contents lists available at ScienceDirect

Journal of the Mechanics and Physics of Solids

journal homepage: www.elsevier.com/locate/jmps

Elastic impact of sphere on large plate

Qing Peng [a,b], Xiaoming Liu [a,b,*], Yueguang Wei [c]

[a] LNM, Institute of Mechanics, Chinese Academy of Sciences, Beijing 100190, China
[b] School of Engineering Science, UCAS, Beijing 100049, China
[c] College of Engineering, Peking University, Beijing 100871, China

ARTICLE INFO

Keywords:
Elastic impact
Homotopy analysis method
Sphere on plate
Coefficient of restitution

ABSTRACT

Different from the Hertz impact, a sphere impacting on a plate has an extra dissipation by the flexural wave propagating on the plate. This wave dissipation has been noticed by Zener (1941), who introduced this dissipation term into the governing equation. Because of this extra dissipation term by the flexural wave, the Zener equation cannot be treated as the same way as in the Hertz impact problem. As a result, in the past 80 years, except few numerical tries for Zener equation, no analytical solution has been provided for the evolution of compressive displacement or contact force during the Zener impact. In this paper, by using homotopy analysis method, we analytically solved the Zener impact problem. After constructing an auxiliary linear operator, we derived an analytical solution for the evolution of contact force up to the first order of the embedding homotopy parameter. Present model can take full account of the elongation of contact time by plate compliance, which is impossible by using Hertz impact model. Comparisons with finite element simulation show that the prediction of the contact force history is of high accuracy. With the solution of force history, we derived an explicit expression for the energy loss of Zener type, this Zener loss has a different dependence on the impact velocity as the Hunter loss does. Also, both the motions of the sphere and the plate are able to be predicted with high accuracy. In addition, with the zeroth-order solution, we derived explicit expressions for both the coefficient of restitution and the contact duration.

1. Introduction

The impact of an elastic sphere to a half-space was first studied by Hertz (1882). In his approach, the system was conservative so that the general form of controlling equation was written as

$$\frac{\mathrm{d}^2\delta}{\mathrm{d}t^2} + k_c\delta^{\frac{3}{2}} = 0 \tag{1}$$

where δ is the displacement of sphere, t the time, and k_c a coefficient depending on the material properties and geometry. By integrating the controlling equation, Hertz obtained an explicit expression for the contact duration given by

* Corresponding author at: LNM, Institute of Mechanics, Chinese Academy of Sciences, Beijing 100190, China.
E-mail address: xiaomingliu@imech.ac.cn (X. Liu).

https://doi.org/10.1016/j.jmps.2021.104604
Received 25 March 2021; Received in revised form 14 June 2021; Accepted 2 August 2021
Available online 8 August 2021

Nomenclature

FEM	finite element method
e	coefficient of restitution
E_1	Young's modulus of sphere
E_2	Young's modulus of plate
E_h	Young's modulus of half-space
E^*	effective modulus
F	contact force
$\overline{F}$	dimensionless contact force
$\overline{F}_m$	maximum dimensionless contact force
$G(\cdot)$	hypergeometric function
H	thickness of plate
I	impulse
$\overline{I}$	dimensionless impulse
k	coefficient in auxiliary linear operator
k_c	coefficient in Hertz's equation of impact
k_{Hunter}	Hunter's coefficient
k_{Reed}	Reed's coefficient
$\mathscr{L}(\cdot)$	auxiliary linear operator
m_1	mass of sphere
m_2	mass of plate
m_h	mass of half-space
m^*	reduced mass
$\mathscr{N}(\cdot)$	nonlinear operator
p	embedding homotopy parameter
R	radius of sphere
t	time
T	characteristic time
T_{Hertz}	Hertz's contact duration
V	velocity of sphere
$\overline{V}$	dimensionless velocity of sphere
V_0	impact velocity
V_W	propagation velocity of quasi-longitudinal waves in plates
w	deflection of plate at center
$\overline{w}$	dimensionless deflection of plate at center
W	energy loss of sphere
α	coefficient in Zener's equation
β	coefficient $\beta = k\lambda/2$
$\Gamma(\cdot)$	gamma function
η	index of asymmetry
δ	compressive relative displacement of sphere and plate
δ_m	maximum compressive relative displacement of sphere and plate
$\overline{\delta}$	dimensionless compressive displacement of sphere and plate
$\overline{\delta}_i$	coefficients in expansion of $\overline{\delta}$ with respect to p
$\overline{\delta}_m$	maximum dimensionless compressive displacement of sphere and plate
ν_1	Poisson's ratio of sphere
ν_2	Poisson's ratio of plate
ν_h	Poisson's ratio of half-space
ξ	ratio of energy loss of sphere
λ	inelasticity parameter
ρ_1	density of sphere
ρ_2	density of plate
τ	dimensionless time
τ_d	dimensionless contact duration
τ_{dc}	dimensionless duration of compression
τ_{dr}	dimensionless duration of recovery
τ_{Hertz}	dimensionless Hertz's contact duration
χ	material-dependent coefficient

ω_0	coefficient $\omega_0 = \sqrt{4k - k^2\lambda^2}/2$

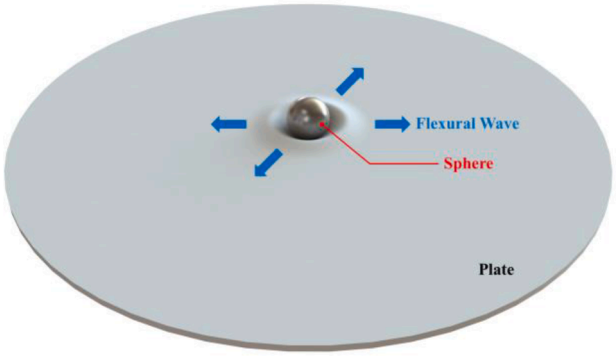

Fig. 1. Schematic diagram for sphere impacting on plate resulting flexural wave as energy loss.

$$T_{\text{Hertz}} = 2.94\left(\frac{15}{16}\frac{m_1 m_h}{m_1 + m_h}\frac{1}{E^*}\right)^{\frac{2}{5}} R_1^{-\frac{1}{5}} V_0^{-\frac{1}{5}} \tag{2}$$

where E^* is the effective modules given by $1/E^* = (1-\nu_1^2)/E_1 + (1-\nu_h^2)/E_h$, m_1 the mass of the sphere, m_h the mass of the half-space, R the radius of the sphere, E_1 the Young's modulus of the sphere, E_h the Young's modulus of the half-space, ν_1 the Poisson's ratio of the sphere, ν_h the Poisson's ratio of the half-space, and V_0 the initial velocity.

Although Eq. (1) neglected the energy dissipation by plasticity or viscosity, Hertz's impact model was widely used to study the energy loss of impact. However, Hertz was not able to give an explicit solution of displacement to Eq. (1). What is more, to authors' knowledge, no explicit solution has been derived so far. Based on Hertz's numerical solution of impact, Hunter studied the energy loss by stress wave in the half-space (often cited as Hunter loss) during the impact. In his approach, he assumed that the history of contact force pulse obeyed the Hertzian impact, and the energy loss was determined by the force pulse over the free surface (Hunter, 1957). Thus, the history of contact force must be known *a priori*.

In lack of explicit expression for the contact force history, Hunter first assumed a history profile for the force pulse by numerically integrating Eq. (1), and then formulated the energy loss by the dynamic response of the half-space due to the assumed force profile on the surface. To complete this formulation, he adopted from Hertz impact solution both the amplitude and the contact period, corresponding to the maximum compressive relative displacement and the contact duration, respectively. The maximum compressive displacement, δ_m, was expressed as:

$$\delta_m = \left(\frac{15}{16}\frac{m_1 m_h}{m_1 + m_h}\frac{1}{E^*}\right)^{\frac{2}{5}} R^{-\frac{1}{5}} V_0^{\frac{4}{5}} \tag{3}$$

By comparing with numerical results of Eq. (1), Hunter found out that sinusoidal profile could provide enough accuracy for the displacement history, expressed as:

$$\delta = \delta_m \sin\left(1.068\frac{V_0}{\delta_m}t\right) \tag{4}$$

As a result, the profile of impact force history, $F(t)$, was determined by Newton's law:

$$F(t) = m_1\ddot{\delta} = -m_1\delta_m\left(1.068\frac{V_0}{\delta_m}\right)^2 \sin\left(1.068\frac{V_0}{\delta_m}t\right) \tag{5}$$

Using this assumption of force history, the Hunter loss, due to stress wave effect as a result of the force pulse on the impact surface of a half-space, was presented explicitly. The predicted coefficient of restitution was compared with experiments by Tillett (1954); agreement for the cases with energy loss less than 5% is well, however, large deviations was found for cases with energy loss more than 5%.

Noticing these deviations, Reed improved Hunter's assumption of the force history. Instead of Newton's law of motion, he used the Hertzian contact law to produce the force history, which in consequence has a sinusoidal profile with a fractional power (Reed, 1985):

$$F(t) = -\frac{4}{3}R^{\frac{1}{2}}E^*\delta_m^{\frac{3}{2}}\sin^{\frac{3}{2}}\left(1.068\frac{V_0}{\delta_m}t\right) \tag{6}$$

With Eq. (6), Reed could provide a more accurate prediction for the impact experiment (Tillett, 1954) than Hunter's model did. The sinusoidal profile or sinusoidal profile with fractional powers were also summarized in the study of the impact of two spheres

(Johnson, 1985), and in the study of the impact between a sphere and a slender beam (Stronge, 2019). Their work showed this approximation was acceptable if only a small fraction of kinetic energy was converted into elastic wave.

These sinusoidal profiles share a common characteristic: symmetry with respect to the time line $t = 1.471\delta_m/V_0$, which means the history of contact force are identical for both compressing stage and recovering stage. In general, the compliance of the structure prolongs the contact duration and reduces the maximum force in any impact (Stronge, 2019). As a result, when the compliance of the structure plays an important part during the impact, the symmetry feature of previous assumption for force profiles (Hunter, 1957; Reed, 1985) cannot hold any more. This viewpoint has been noticed by Lee in the study the impact of a sphere on a very slender beam (Lee, 1940), the compliance of the beam elongates the contact duration, and thus the sinusoidal profile is obviously no longer correct. Such symmetry break by compliance was also noticed in the classic book on impact dynamics (Stronge, 2019). However, till now, there is still no analytical solution to consider the structure compliance.

The Hunter's treatment is more like a one-way coupling approach: the contact pulse determines the energy loss by stress wave propagating in the half-space, but the contact pulse is not affected by the stiffness of the half-space. This assumption can be accepted for a half-space in some cases, but for the structure with high compliance such as a beam or a plate, large deviation may appear and thus a correct model considering the compliance of structure is required.

For the elastic impact of a sphere on a flexible structure, for example, a plate, the energy loss comprises of not only the Hunter loss but also a secondary loss due to the flexural oscillations on the plate, illustrated by Fig. 1. When the diameter-to-thickness ratio exceeds 0.2, Koller showed that the prediction by Hunter's model deviates from experiments (Koller and Kolsky, 1987). In such case, the flexural wave must be considered and the compliance of the plate, similar to the compliance of a beam, can significantly elongate the duration of recovery and break the symmetrical sinusoidal assumption (Zener, 1941). As a result, such process can hardly be explained with the theories by Hunter (1957), Aboudi (1978), Hutchings (1979), or Reed (1985).

To model the impact on a flexible plate, Zener derived a coupled controlling equation depending on an inelasticity parameter λ. In his model, the plate was sufficiently large such that the impacting process was not affected by the reflected flexural wave from the boundary. With numerical solution, Zener obtained a relationship of the COR e with λ; the result showed good agreement with Raman's experiments (Raman, 1920) and later confirmed by another experiments (Tillett, 1954). However, until now, we have not found any analytical solution for Zener's equation except for some linearization approaches in the literature. For example, Mueller et al. (2015) replaced the nonlinear contact law with a linear one and hence obtained an approximated solution, which can agree well for $\lambda < 0.85$ and $e > 0.2$. Such linearization method was used to study the contact time (Muller et al., 2016) and the energy dissipation (Boettcher et al., 2017b).

For the Hertz impact of a sphere on a half space, Hunter has proposed a sinusoidal profile to fit Eq. (1). Recently, for the Zener impact of a sphere on a thick plate, Boettcher et al. recalculated the model of Hunter using Reed's more accurate force-time approximation, obtaining more accurate results (Boettcher et al., 2017a). For general cases, which includes the cases with large λ, similar to Hunter's approach, we tried to seek a force profile which fits Zener's numerical solution. Unlike the treatment by Hunter (1957) and Reed (1985), as λ varies, the breaking of symmetry leads to that no universal representative function could represent the history of Zener's impact force so far.

The symmetry of contact force history will also break due to contact plasticity (Lifshitz and Kolsky, 1964; Patil and Higgs, 2017; Stronge, 2000; Thornton, 1997; Wu et al., 2003, 2005), contact adhesion (Ciavarella et al., 2019; Feng et al., 2009; Peng et al., 2020; Thornton et al., 2017), and contact viscosity (Flores et al., 2011; Hunter, 1960; Lankarani and Nikravesh, 1990; Maier and Tsai, 1974). For example, on the study of high-speed elastoplastic impact of a sphere on a half-space, Hutchings showed that asymmetrical force history was evident; Hutchings combined sinusoidal and cosinusoidal profiles with different periods for the loading and unloading of contact force, respectively (Hutchings, 1979). In addition, plasticity-induced asymmetry was also noticed in our previous study (Peng et al., 2021). These plastic or viscous situations often imply high-speed impacts or viscous materials, and thus the Hertzian contact law can hardly be used to establish the controlling equation.

In sum, the breaking of symmetry by compliance has been noticed for almost 80 years, but either the profile of contact force history has not been provided universally, or the assumed profiles lack of theoretical foundation. In this paper, we analytically solved Zener's equation using homotopy analysis method. After constructing an auxiliary linear operator, we derived an analytical solution for the contact force history up to the first order of the embedding homotopy parameter. With the force solution, we studied the energy loss of Zener type impact theoretically and proposed a semi-analytical model. Further, the motion of sphere, the deflection of plate, and the coefficient of restitution were also investigated; finite element simulations were also carried out to verify the proposed solution.

2. Solving Zener's equation via homotopy analysis method

2.1. Zener's equation

Considering the flexural vibration of plate due to a point load, Zener derived the controlling equation to model the elastic impact between a sphere and a plate. Assuming the plate is sufficiently large, he thus ignored the effect of reflected flexural wave from the boundary. The controlling equation was:

$$\frac{\mathrm{d}^2\delta}{\mathrm{d}t^2} + \frac{F(\delta)}{m^*} + \alpha\frac{\mathrm{d}}{\mathrm{d}t}F(\delta) = 0 \tag{7}$$

with initial conditions:

$$\begin{cases} \delta|_{t=0} = 0 \\ \dot{\delta}|_{t=0} = V_0 \end{cases}$$

where V_0 is the initial velocity of the sphere, δ the compressive displacement during contact, $\dot{\delta}$ the time derivative of δ, m^* the reduced mass determined by $m^{*-1} = m_1^{-1} + m_2^{-1}$, m_1 the mass of the sphere, m_2 the mass of the plate, t the time, α a constant expressed by

$$\alpha = \frac{1}{4\rho_2 H^2}\sqrt{\frac{3\rho_2(1-\nu_2^2)}{E_2}}$$

ρ_2 the density of the plate, E_2 the Young's modulus of the plate, ν_2 the Poisson's ratio of the plate, H the thickness of the plate, and F the contact force between the two objects that uniquely determined by the compressive displacement δ. For an impact with small compressive displacement, the Hertzian contact model was adopted:

$$F(\delta) = \frac{4}{3}E^* R^{\frac{1}{2}}\delta^{\frac{3}{2}} \tag{8}$$

where E^* is the effective modulus given by $1/E^* = (1-\nu_1^2)/E_1 + (1-\nu_2^2)/E_2$, ν_1 the Poisson's ratio of the sphere, E_1 the Young's modulus of the sphere. By introducing dimensionless compressive displacement $\overline{\delta}$ and dimensionless time τ as follows

$$\begin{cases} \overline{\delta} = \dfrac{\delta}{TV_0} \\ \tau = \dfrac{t}{T} \end{cases} \tag{9}$$

where T is a characteristic time given by

$$T = \left(\frac{m^*}{\frac{4}{3}E^*\sqrt{RV_0}}\right)^{\frac{2}{5}}$$

In this manner, the dimensionless Hertz's contact duration can be calculated by substituting Eq. (9) to Eq. (2): $\tau_{\text{Hertz}} \approx 3.214$. Eq. (7) can be transformed to the following dimensionless form

$$\frac{\mathrm{d}^2\overline{\delta}}{\mathrm{d}\tau^2} + \left(1 + \lambda\frac{\mathrm{d}}{\mathrm{d}\tau}\right)\overline{\delta}^{\frac{3}{2}} = 0 \tag{10}$$

with initial conditions

$$\begin{cases} \overline{\delta}|_{\tau=0} = 0 \\ \dot{\overline{\delta}}|_{\tau=0} = 1 \end{cases}$$

where λ is the inelasticity parameter or relative compliance given by

$$\lambda = \frac{\pi^{\frac{3}{5}}}{3^{\frac{1}{5}}}\left(\frac{R}{H}\right)\Big\langle ce{:}textref{>}LalanneM.,BerthierP.,DerHagopianJ.,(1983).{<}ce{:}inter{-}refid{=}"interref0002"xlink{:}href{=}"https{:}//cel.archives{-}ouvertes.fr/cel{-}00315803"{>}https{:}//cel.archives{-}ouvertes.fr/cel{-}00315803{</}ce{:}inter{-}ref{>}.{</}ce{:}textref{><}/ce{:}other{-}ref{>}{<}/ce{:}bib{-}reference{>}\Big\rangle^2\left(\frac{V_0}{V_W}\right)^{\frac{1}{5}}\left(\frac{\rho_1}{\rho_2}\right)^{\frac{3}{5}}\left(\frac{E_1/(1-\nu_1^2)}{E_1/(1-\nu_1^2)+E_2/(1-\nu_2^2)}\right)^{\frac{2}{5}} \tag{11}$$

and $V_W = \sqrt{E_2/\rho_2(1-\nu_2^2)}$ is the propagation velocity of quasi-longitudinal waves in thin plates (Landau et al., 1986).

2.2. The homotopy analysis method

Because of the fractional ordered term $\overline{\delta}^{\frac{3}{2}}$, the Zener equation, Eq. (10), cannot be solved in a traditional way. As a result, till now, we have not found any theoretical solution to the Zener model. In this section, we use homotopy analysis method to solve Eq. (10). Unlike traditional perturbation method (Nayfeh, 2000), homotopy analysis method does not depend on small parameter and thus can provide an effective way to solve a wide range of nonlinear problems (Liao, 2012, 2014); Liao's group is pioneer group in this field, they proposed this method in 1990s, and further extended by researchers in other fields. For example, Abbasbandy used homotopy analysis method to solve the problem of cooling of a lumped system with variable specific heat (Abbasbandy, 2006), and nonlinear problems concerning solitary waves (Abbasbandy, 2007, 2008). Yabushita et al. (2007) obtained an analytical solution of projectile motion with the quadratic resistance law using the homotopy analysis method; the equations of motion for this case with a general

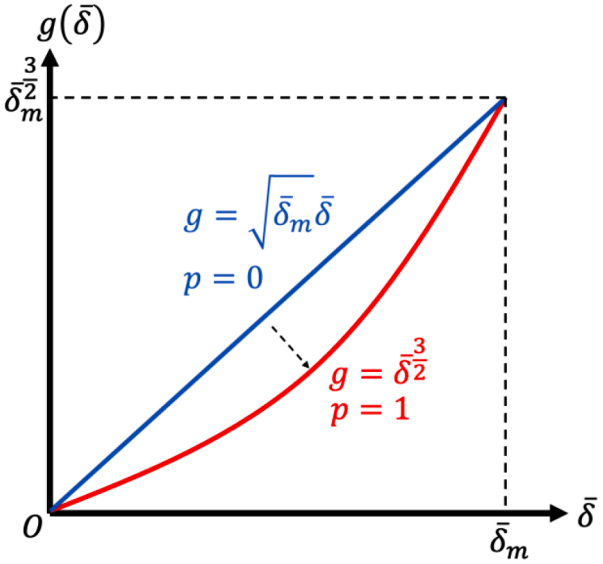

Fig. 2. Geometric view of continuous deformation for present differential equation.

projectile angle had been considered unsolvable.

By introducing the maximal dimensionless compressive displacement $\bar{\delta}_m$ that determined by Eq. (10) and using the homotopy analysis approach, we define the following linear and nonlinear operators:

$$\mathscr{L}(\bar{\delta}) = \frac{\mathrm{d}^2\bar{\delta}}{\mathrm{d}\tau^2} + \left(1 + \lambda\frac{\mathrm{d}}{\mathrm{d}\tau}\right)k\bar{\delta} \tag{12}$$

$$\mathscr{N}(\bar{\delta}) = \frac{\mathrm{d}^2\bar{\delta}}{\mathrm{d}\tau^2} + \left(1 + \lambda\frac{\mathrm{d}}{\mathrm{d}\tau}\right)\bar{\delta}^{\frac{3}{2}} \tag{13}$$

where $k = \sqrt{\bar{\delta}_m}$. We construct the zero-order deformation equation

$$(1-p)\mathscr{L}(\bar{\delta}) + p\mathscr{N}(\bar{\delta}) = 0 \tag{14}$$

or identically,

$$(1-p)(\ddot{\bar{\delta}} + k\lambda\dot{\bar{\delta}} + k\bar{\delta}) + p\left(\ddot{\bar{\delta}} + \frac{3}{2}\lambda\sqrt{\bar{\delta}}\dot{\bar{\delta}} + \bar{\delta}^{\frac{3}{2}}\right) = 0 \tag{15}$$

where $p \in [0,1]$ is the embedding homotopy parameter, $\ddot{\bar{\delta}} = \frac{\mathrm{d}^2\bar{\delta}}{\mathrm{d}\tau^2}$, and $\dot{\bar{\delta}} = \frac{\mathrm{d}\bar{\delta}}{\mathrm{d}\tau}$. Particularly, from $p = 0$ to $p = 1$, the term of contact force continuously deforms from the linear pattern $k\bar{\delta}$ to the desired nonlinear pattern $\bar{\delta}^{3/2}$, shown in Fig. 2. For Eq. (14), we assume that the solution can be written as

$$\bar{\delta} = \bar{\delta}_0 + \sum_{i=1}^{\infty}\bar{\delta}_i p^i \tag{16}$$

so that the solution $\bar{\delta}$ can deform continuously from the solution of $\mathscr{L}(\bar{\delta}) = 0$ to that of $\mathscr{N}(\bar{\delta}) = 0$ as p varies from 0 to 1.

2.3. Construction of the auxiliary linear operator

To complete the auxiliary operator $\mathscr{L}(\bar{\delta})$, we have to determine the relationship between $\bar{\delta}_m$ and λ. First of all, we transform Eq. (10) into a first-order differential equation by setting $y = \dot{\bar{\delta}}$:

$$y\frac{\mathrm{d}y}{\mathrm{d}\bar{\delta}} + \frac{3}{2}\lambda\sqrt{\bar{\delta}}y + \bar{\delta}^{\frac{3}{2}} = 0 \tag{17}$$

Then, $\bar{\delta}_m$ can be solved by finding the root of $y(\bar{\delta}) = 0$, where $y(\bar{\delta})$ is the solution to Eq. (17). Although Eq. (17) is unsolvable directly, we can adopt an asymptote approach to check the solution $y(\bar{\delta})$ for the cases of $\lambda \to \infty$ and $\lambda \to 0$.

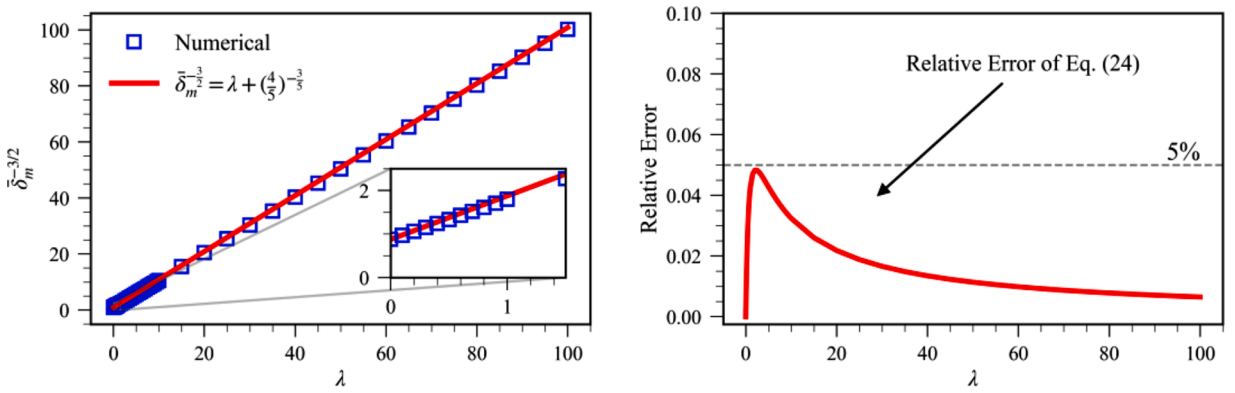

Fig. 3. A) $\bar{\delta}_m$ as a function of λ. B) Relative error of Eq. (24) to results of numerical solution of Eq. (10).

- As $\lambda \to \infty$, Eq. (17) can be approximated by

$$\frac{dy}{d\bar{\delta}} + \frac{3}{2}\lambda\sqrt{\bar{\delta}} = 0 \tag{18}$$

Solution to Eq. (18) can be obtained by direct integration

$$y = 1 - \lambda\bar{\delta}^{\frac{3}{2}} \tag{19}$$

As a result, we have the relationship between $\bar{\delta}_m$ and λ for $\lambda \to \infty$ as follows:

$$\bar{\delta}_m^{-\frac{3}{2}} = \lambda, \text{ as } \lambda \to \infty \tag{20}$$

- As $\lambda \to 0$, Eq. (17) becomes

$$y\frac{dy}{d\bar{\delta}} + \bar{\delta}^{\frac{3}{2}} = 0 \tag{21}$$

Solution to Eq. (21) can be expressed by

$$y = \sqrt{1 - \frac{4}{5}\bar{\delta}^{\frac{5}{2}}} \tag{22}$$

Hence, we obtain the maximum of $\bar{\delta}$ for $\lambda \to 0$

$$\bar{\delta}_m = \left(\frac{5}{4}\right)^{\frac{2}{5}}, \text{ as } \lambda \to 0 \tag{23}$$

Combining Eqs. (20) and (23), we construct the following expression for $\bar{\delta}_m$ with respect to λ as a first-order approximation:

$$\bar{\delta}_m^{-\frac{3}{2}} = \lambda + \left(\frac{5}{4}\right)^{-\frac{3}{5}} \tag{24}$$

Next, we exam the validity of Eq. (24). By solving Eq. (10) numerically with Runge-Kutta method (Dormand and Prince, 1980; Shampine, 1986), a numerical relationship between $\bar{\delta}_m^{-\frac{3}{2}}$ and λ can be obtained, shown in Fig. 3(A). For $\lambda \in [0,\ 100]$ ($\lambda \leq 2$ in most cases (Mueller et al., 2015; Zener, 1941), the present first-order relationship Eq. (24) can be used for the estimation of $\bar{\delta}_m^{-\frac{3}{2}}$, with a maximum error less than 5%.

In sum, we construct the following expression for the coefficient k in $\mathscr{L}(\bar{\delta}) = 0$.

$$k = \sqrt{\bar{\delta}_m} = \left(\lambda + \left(\frac{5}{4}\right)^{-\frac{3}{5}}\right)^{-\frac{1}{3}} \tag{25}$$

2.4. Solution to Zener's equation

We seek a solution up to the first order of p in Eq. (16). Using Taylor's expansion for $\sqrt{\bar{\delta}}$ and $\bar{\delta}^{\frac{3}{2}}$ at $\bar{\delta} = \bar{\delta}_0$, i.e.

$$\sqrt{\bar{\delta}_0 + p\bar{\delta}_1} = \sqrt{\bar{\delta}_0} + \frac{1}{2}\frac{\bar{\delta}_1}{\sqrt{\bar{\delta}_0}}\, p - \frac{1}{8}\frac{\bar{\delta}_1^2}{\bar{\delta}_0^{1.5}}p^2 + \ldots \tag{26}$$

and

$$\left(\bar{\delta}_0 + p\bar{\delta}_1\right)^{\frac{3}{2}} = \bar{\delta}_0^{\frac{3}{2}} + \frac{3}{2}\sqrt{\bar{\delta}_0}p + \frac{3}{8}\frac{\bar{\delta}_1^2}{\sqrt{\bar{\delta}_0}}p^2 + \ldots \tag{27}$$

substituting Eqs. (16), (26) and (27) into Eq. (14), and collecting terms respect to p^n, we have the following equation for $\bar{\delta}_0$

$$\ddot{\bar{\delta}}_0 + k\lambda\dot{\bar{\delta}}_0 + k\bar{\delta}_0 = 0 \tag{28}$$

with initial conditions:

$$\begin{cases} \bar{\delta}_0(0) = 0 \\ \dot{\bar{\delta}}_0 \end{cases}(0) = 1 \tag{29}$$

and the following equation for $\bar{\delta}_1$

$$\ddot{\bar{\delta}}_1 + k\lambda\dot{\bar{\delta}}_1 + k\bar{\delta}_1 = -\left(\ddot{\bar{\delta}}_0 + \frac{3}{2}\lambda\sqrt{\bar{\delta}_0}\,\dot{\bar{\delta}}_0 + \bar{\delta}_0^{\frac{3}{2}}\right) \tag{30}$$

with initial conditions:

$$\begin{cases} \bar{\delta}_1(0) = 0 \\ \dot{\bar{\delta}}_1(0) = 0 \end{cases} \tag{31}$$

The characteristic equation of Eq. (28) is:

$$x^2 + k\lambda x + k = 0$$

and has the following solution

$$x_{1,2} = -\frac{k\lambda}{2} \pm \frac{\sqrt{4k - k^2\lambda^2}}{2}i$$

Here, we only interested in the range $\lambda \le 2/\sqrt{k}$ such that the coefficient of restitution is larger than 0 (Mueller et al., 2015). Introducing

$$\beta = \frac{k\lambda}{2} = \frac{\lambda}{2}\left(\lambda + \left(\frac{5}{4}\right)^{-\frac{3}{5}}\right)^{-\frac{1}{3}} \tag{32}$$

and

$$\omega_0 = \frac{\sqrt{4k - k^2\lambda^2}}{2} = \frac{\sqrt{4\left(\lambda + \left(\frac{5}{4}\right)^{-\frac{3}{5}}\right)^{-\frac{1}{3}} - \lambda^2\left(\lambda + \left(\frac{5}{4}\right)^{-\frac{3}{5}}\right)^{-\frac{2}{3}}}}{2} \tag{33}$$

the general solution has the following form.

$$\bar{\delta}_0 = \exp(-\beta\tau)(c_1\sin(\omega_0\tau) + c_2\cos(\omega_0\tau)) \tag{34}$$

where c_1 and c_2 are constant coefficient to be determined. Substituting the initial condition Eq (29) to Eq. (34), we obtain $c_1 = \omega_0^{-1}$ and $c_2 = 0$. Hence the solution can be expressed as follows.

$$\bar{\delta}_0(\tau) = \frac{1}{\omega_0}\exp(-\beta\tau)\sin(\omega_0\tau) \tag{35}$$

Substituting Eq. (35) into Eq. (30), we obtain the equation for $\bar{\delta}_1$

$$\begin{aligned}\ddot{\bar{\delta}}_1 + k\lambda\dot{\bar{\delta}}_1 + k\bar{\delta}_1 = &\frac{\omega_0^2-\beta^2}{\omega_0}\exp(-\beta\tau)\sin(\omega_0\tau) + 2\beta\exp(-\beta\tau)\cos(\omega_0\tau)\\ &-\frac{3}{2}\lambda\sqrt{\frac{1}{\omega_0}}\exp\left(-\frac{3\beta\tau}{2}\right)\sin^{\frac{1}{2}}(\omega_0\tau)\cos(\omega_0\tau)\\ &+\left(\frac{3}{2}\lambda\beta-1\right)\left(\frac{1}{\omega_0}\right)^{\frac{3}{2}}\exp\left(-\frac{3\beta\tau}{2}\right)\sin^{\frac{3}{2}}(\omega_0\tau)\end{aligned} \tag{36}$$

Eq. (36) can be solved by the method of constant variation (Hille, 1968). We assume the solution to Eq. (36) can be expressed as follows

$$\bar{\delta}_1 = \exp(-\beta\tau)(C_{11}(\tau)\sin(\omega_0\tau) + C_{12}(\tau)\cos(\omega_0\tau)) \tag{37}$$

where $C_{11}(\tau)$ and $C_{12}(\tau)$ are coefficients to be determined. Substituting Eq. (37) to Eq. (36) and employing the procedures of the method of constant variation, we obtain the following equations to determine $C_{11}(\tau)$ and $C_{12}(\tau)$.

$$\begin{cases} C_{11}'(\tau)\sin(\omega_0\tau) + C_{12}'(\tau)\cos(\omega_0\tau) = 0\\ C_{11}'(\tau)\cos(\omega_0\tau) - C_{12}'(\tau)\sin(\omega_0\tau) = \dfrac{1}{\omega_0}e^{\beta\tau}f(\tau)\end{cases} \tag{38}$$

where $f(\tau)$ is the right-hand side of Eq. (36). Solving Eq. (38), we have

$$\begin{cases} C_{11}'(\tau) = \dfrac{\cos(\omega_0\tau)}{\omega_0}e^{\beta\tau}f(\tau)\\ C_{12}'(\tau) = -\dfrac{\sin(\omega_0\tau)}{\omega_0}e^{\beta\tau}f(\tau)\end{cases} \tag{39}$$

Integrating Eq. (39) term by term, we obtain

$$C_{11}(\tau) = \frac{\omega_0^2-\beta^2}{\omega_0^2}C_{111} + \frac{2\beta}{\omega_0}C_{112} - \frac{3\lambda}{2\omega_0^{\frac{3}{2}}}C_{113} + \frac{(3\lambda\beta-2)}{2\omega_0^{\frac{5}{2}}}C_{114} \tag{40}$$

where

$$C_{111} = -\frac{\cos^2(\omega_0\tau)}{2\omega_0}$$

$$C_{112} = \frac{\tau}{2} + \frac{\sin(2\omega_0\tau)}{4\omega_0}$$

$$\begin{aligned}C_{113} = &\frac{1}{2\left(\beta^2+25\omega_0^2\right)}\left(2e^{-\frac{1}{2}\beta\tau}\sqrt{\sin(\omega_0\tau)}(\beta\cos(2\omega_0\tau) - 5\omega_0\sin(2\omega_0\tau)) - \frac{(1+i)e^{-\frac{1}{2}\tau(\beta+i\omega_0)}}{(\beta+i\omega_0)(\beta-3i\omega_0)}\right.\\ &\left.\left(\left(\beta^3-4i\beta^2\omega_0+17\beta\omega_0^2-60i\omega_0^3\right)G\left(\frac{1}{2},\frac{i\beta}{4\omega_0}-\frac{1}{4},\frac{i\beta}{4\omega_0}+\frac{3}{4};e^{2i\omega_0\tau}\right) - \left(\beta^3+2i\beta^2\omega_0+19\beta\omega^2+20i\omega_0^3\right)e^{2i\omega_0\tau}G\left(\frac{1}{2},\frac{i\beta}{4\omega_0}+\frac{3}{4},\frac{i\beta}{4\omega_0}+\frac{7}{4};e^{2i\omega_0\tau}\right)\right)\right)\end{aligned}$$

$$\begin{aligned}C_{114} = &\frac{\sqrt{\sin(\omega_0\tau)}\quad \omega_0 e^{-\frac{\beta}{2}\tau}}{\beta^2+25\omega_0^2\ (\beta+i\omega_0)(\beta-3i\omega_0)}\left(\left(-\beta^2+8i\beta\omega_0+15\omega_0^2\right)G\left(1,\frac{i\beta}{4\omega_0}+\frac{1}{4},\frac{i\beta}{4\omega_0}+\frac{3}{4};e^{2i\omega_0\tau}\right) + e^{2i\omega_0\tau}\left(\beta^2+6i\beta\omega_0-5\omega_0^2\right)\right.\\ &\left.G\left(1,\frac{i\beta}{4\omega_0}+\frac{5}{4},\frac{i\beta}{4\omega_0}+\frac{7}{4};e^{2i\omega_0\tau}\right)\right)\beta e^{-\frac{\beta}{2}\tau}\sin(2\omega_0\tau) - 5\omega_0 e^{-\frac{\beta}{2}\tau}\cos(2\omega_0\tau)\Bigg)\end{aligned}$$

$G(\cdot)$ is the hypergeometric function (Arfken et al., 2013) (here we use notion $G(\cdot)$ instead of the commonly used ${}_2F_1(\cdot)$ to avoid ambiguity) and

$$C_{12}(\tau) = -\frac{\omega_0^2-\beta^2}{\omega_0^2}C_{121} - \frac{2\beta}{\omega_0}C_{122} + \frac{3\lambda}{2\omega_0^{\frac{3}{2}}}C_{123} - \frac{(3\lambda\beta-2)}{2\omega_0^{\frac{5}{2}}}C_{124} \tag{41}$$

where

$$C_{121} = \frac{\tau}{2} - \frac{\sin(2\omega_0\tau)}{4\omega_0}$$

$$C_{122} = C_{111}$$

$$C_{123} = C_{114}$$

$$C_{124} = \frac{2e^{-\frac{\beta}{2}\tau}(e^{2i\omega_0\tau}-1)}{\beta+5i\omega_0}\sin^{\frac{5}{2}}(\omega_0\tau)G\left(1, \frac{i\beta}{4\omega_0}+\frac{9}{4}; \frac{i\beta}{4\omega_0}-\frac{1}{4}; e^{2i\omega_0\tau}\right)$$

Finally, we obtain the solution to Eq. (10) up to the first order of the embedding homotopy parameter p as follows.

$$\bar{\delta}\& = \bar{\delta}_0 + \bar{\delta}_1 = \frac{1}{\omega_0}\exp(-\beta\tau)\sin(\omega_0\tau) + (C_{11}(\tau) - C_{11}(0))e^{-\beta t}\sin(\omega_0\tau) + (C_{12}(\tau) - C_{12}(0))e^{-\beta t}\cos(\omega_0\tau) \tag{42}$$

where, explicitly,

$$C_{11}(0) = \frac{(\beta^2-\omega_0^2)}{2\omega_0^3} + \frac{3(1-i)\lambda\sqrt{\pi}(\beta^2+10\omega_0^2)\Gamma\left(\frac{i\beta}{4\omega_0}-\frac{5}{4}\right)}{256\omega_0^{\frac{9}{2}}\Gamma\left(\frac{i\beta}{4\omega_0}+\frac{9}{4}\right)}$$

$$C_{12}(0) = \frac{\beta}{\omega_0^2}$$

and $\Gamma(\cdot)$ is the gamma function (Arfken et al., 2013).

3. Results and discussion

Using the explicit expressions, Eqs. (35) and (42), we can obtain the contact force history, with which the feature of asymmetry will be checked in the section. Further, the contact force history can be used to calculate the motions of sphere and plate, and in turn the energy loss of Zener type. This section is organized as follows: first, we formulate the contact forces based on the displacement variation during the impact; second, we compare the present contact force history with the one in Hertz's impact theory when the compliance of plate is very small (thick plate); third, we check the effect of compliance on the contact force, the motions of sphere and plate, and the energy loss; last, based on the zeroth-order solution, we derive an explicit expression for the coefficient of restitution.

3.1. Formulation of force and impulse

In this section, we formulate the contact force based on the present solutions Eqs. (35) and (42). With Eqs. (8) and (9), we can write the contact force as a function of $\bar{\delta}$:

$$F = \left(\frac{4}{3}E^*R^{\frac{1}{2}}\right)^{\frac{2}{5}} m^{*\frac{3}{5}} V_0^{\frac{6}{5}} \bar{\delta}^{\frac{3}{2}} \tag{43}$$

We introduce a dimensionless force, $\bar{F}$, as follows,

$$\bar{F} = \frac{F}{\left(\frac{4}{3}E^*R^{\frac{1}{2}}\right)^{\frac{2}{5}} m^{*\frac{3}{5}} V_0^{\frac{6}{5}}} \tag{44}$$

so that

$$\bar{F} = \bar{\delta}^{\frac{3}{2}} \tag{45}$$

or explicitly, for zeroth-order solution

$$\bar{F} = \left(\frac{1}{\omega_0}\exp(-\beta\tau)\sin(\omega_0\tau)\right)^{\frac{3}{2}}$$

and for first-order solution

$$\bar{F} = \left(\frac{1}{\omega_0}\exp(-\beta\tau)\sin(\omega_0\tau) + (C_{11}(\tau) - C_{11}(0))e^{-\beta t}\sin(\omega_0\tau) + (C_{12}(\tau) - C_{12}(0))e^{-\beta t}\cos(\omega_0\tau)\right)^{\frac{3}{2}}$$

The impulse by F during a time interval can be expressed as

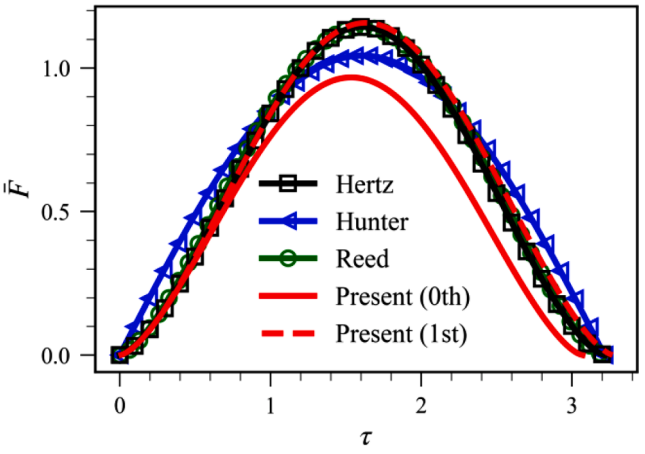

Fig. 4. Comparison of present solutions to various models for Hertzian impact ($\lambda = 0$).

$$I = \int_0^t F(t')\mathrm{d}t' \tag{46}$$

The dimensionless form of Eq. (46) is then

$$\bar{I} = \int_0^\tau \bar{F}(\tau')\mathrm{d}\tau' \tag{47}$$

so that

$$\bar{I} = \frac{I}{m^* V_0} \tag{48}$$

With Eqs. (43)–(45), we present the history of contact force. Further, considering the accumulated effect of the contact force over time, we present the expression of impulse as in Eqs. (46)–(48).

3.2. *Comparing present solution to Hertz's impact theory for a thick plate*

In particular, the value of λ approaches to zero for a thick plate. In this case, the contact force history should be consistent with the analysis of Hertz (1882) and Love (1944). The dimensionless compressive displacement can be written as

$$\bar{\delta} = \underbrace{\frac{\sin(\omega_0\tau)}{\omega_0}}_{\bar{\delta}_0} + \underbrace{\frac{\sin(\omega_0\tau)}{2\omega_0} + C_{11}^d(\tau)\sin(\omega_0\tau) + C_{12}^d(\tau)\cos(\omega_0\tau)}_{\bar{\delta}_1} \tag{49}$$

where $\omega_0 = \left(\frac{5}{4}\right)^{\frac{1}{10}} \approx 1.023$ and

$$C_{11}^d(\tau) = -\frac{\cos^2(\omega_0\tau)}{2\omega_0} - \frac{2}{5\omega_0}\left(\frac{\sin(\omega_0\tau)}{\omega_0}\right)^{\frac{5}{2}}$$

$$C_{12}^d(\tau) = \frac{\sin(2\omega_0\tau) - 2\omega_0\tau}{4\omega_0} - \frac{4}{5}e^{i\omega_0\tau}G\left(1, \frac{9}{4}; -\frac{1}{4}; e^{2i\omega_0\tau}\right)\left(\frac{\sin(\omega_0\tau)}{\omega_0}\right)^{\frac{7}{2}}$$

As a result, the expressions for $\bar{F}$ for $\lambda = 0$ are as follows.
For the zeroth-order solution:

$$\bar{F} = \left(\frac{\sin(1.023\tau)}{1.023}\right)^{\frac{3}{2}} = 0.966\sin^{\frac{3}{2}}(1.023\tau) \tag{50}$$

and for the first-order solution:

$$\bar{F} = \left(1.467\sin(1.023\tau) + C_{11}^d(\tau)\sin(1.023\tau) + C_{12}^d(\tau)\cos(1.023\tau)\right)^{\frac{3}{2}} \tag{51}$$

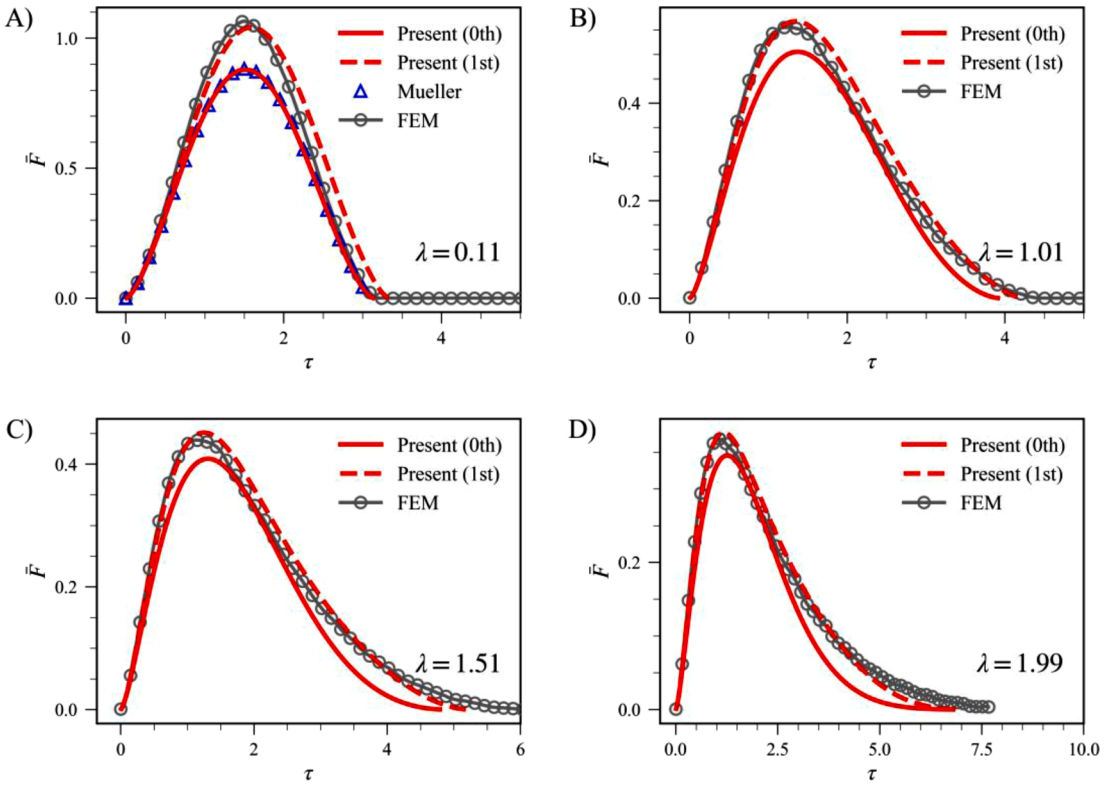

Fig. 5. History of contact force for the case of A) $\lambda = 0.11$, B) $\lambda = 1.01$, C) $\lambda = 1.51$, and D) $\lambda = 1.99$.

For comparison, Hunter's expression for the contact force can be obtained by substituting Eqs. (3) and (44) to Eq. (5):

$$\overline{F}_{\text{Hunter}} = 1.043\sin(0.977\tau) \tag{52}$$

Similarly, Reed's expression can also be obtained:

$$\overline{F}_{\text{Reed}} = 1.143\sin^{\frac{3}{2}}(0.977\tau) \tag{53}$$

On one hand, compared with the numerical solution of Hertz, among Eqs. (50)–(53), the present first-order solution and Reed's solution show little deviation, as shown in Fig. 4. The first-order solution can be degraded to Hertz's solution as $\lambda \to 0$. On the other hand, all solutions are strictly symmetrical in the case of $\lambda = 0$, but only the present solutions can account for the effect of the compliance of plate. In the following section, we show how the compliance affects the contact force history.

3.3. *Effects of compliance on the contact force history*

To study the effect of the compliance on the history of contact force, we check how λ affects the present solutions. We also verified present solution with finite element simulations, where we took an elastic sphere (γAl_2O_3) impacting a sufficiently large elastic plate (glass) as an example. Details are provided in Appendix.

The comparison between the present solutions and the FEM simulations is shown by Fig. 5, in which we also plot Mueller's linearized solution (Mueller et al., 2015). Mueller's model can provide high accuracy for $\lambda < 0.85$; In this range, the present 0th solution agree well with Mueller's solution. Mueller's solution can not be used for $\lambda > 0.85$. Compared with the FEM results, on one hand, the present first-order solution agrees very well as shown in Fig. 5. Also, the present zeroth-order solution approximates to the FEM results when λ increases to larger than one. For a small λ, for example $\lambda = 0.11$, the contact force history is almost symmetrical, shown by Fig. 5(A). As λ increases, the symmetry of contact force breaks, shown by Fig. 5(B–D), rendering the profiles by Hunter and Reed invalid. The reason for such symmetry break is the exponential term in Eq. (35), which originates from the compliance term $\lambda \frac{\mathrm{d}}{\mathrm{d}\tau}\overline{\delta}^{\frac{3}{2}}$ in Zener's equation Eq. (10). Compared with Hertz's impact as shown in Fig. 4, the compliance of plate accounts for an additional drag to the relative motion of contact, which leads to a shortened compression and a prolonged recovery; the larger the compliance is, the longer the recovery process will take. From above, we can conclude that the compliance of plate is the sole reason for breaking the symmetric feature of the contact force history.

To show how much the compliance affects the contact force history, we investigate the maximum force, the contact duration as an indicator of the contact force asymmetry, and the impulse as an accumulated effect over time.

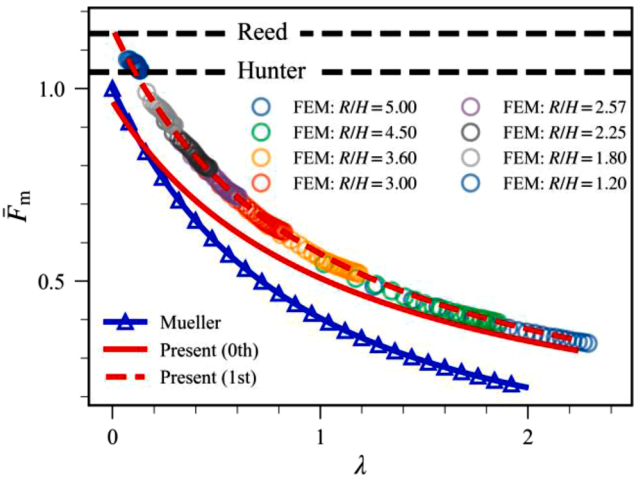

Fig. 6. Maximum dimensionless contact force as function of inelasticity parameter λ

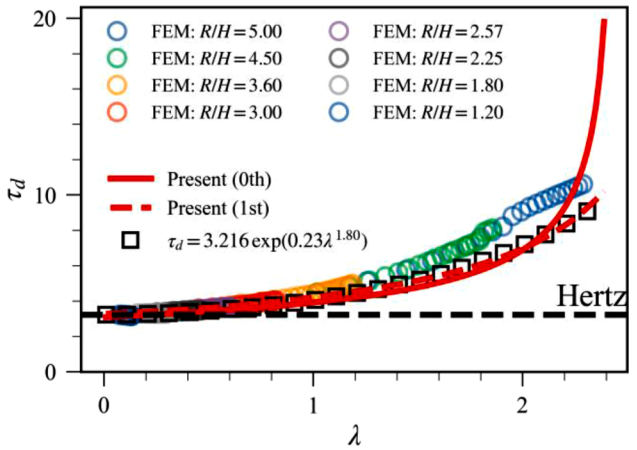

Fig. 7. Dimensionless contact duration as function of inelasticity parameter λ.

The dependency of the maximum contact force on λ is shown in Fig. 6, in which we also plot the relationship by Mueller's, Hunter's, and Reed's models for comparison. First of all, larger compliance of the plate (thinner plate) leads to more energy dissipated by the flexural wave, resulting in less compressive force. Second, Mueller's model always underestimates $\overline{F}_m$, with the relative error up to 38.72%; while the present first-order solution can predict the maximum contact force with a relative error less than 2.90%. The present zeroth-order solution can provide an estimation of $\overline{F}_m$ with relative error less than 5.11%, but only for the case of $\lambda > 1.5$.

Also, we check the effect of compliance on the contact duration. By equating the first-order solution Eq. (42) to zero, we can derive an implicit equation for the contact duration; with numerical procedure, we can obtain the relationship between the contact duration and λ. Fig. 7 shows the contact duration as a function of λ according to the present solutions. In addition, the zeroth-order solution can provide an explicit expression for the contact duration, as follows.

$$\tau_d = \frac{\pi}{\omega_0} = \frac{2\pi}{\sqrt{4\left(\lambda + \left(\frac{5}{4}\right)^{-\frac{3}{5}}\right)^{-\frac{1}{5}} - \left(\lambda + \left(\frac{5}{4}\right)^{-\frac{3}{5}}\right)^{-\frac{2}{3}}\lambda^2}} \tag{54}$$

For $\lambda = 0$, we can calculate that $\tau_d \approx 3.072$, which is close to the dimensionless Hertz's contact duration $\tau_{\text{Hertz}} \approx 3.214$. The predictions by first-order and zero-order solutions are confirmed by the FEM simulation, showing that the compliance of plate prolongs contact process: a greater value of λ leads to a longer contact duration.

In lack of explicit expression based on the first-order solution, we can alternatively use an exponential function to fit the results, which has the form:

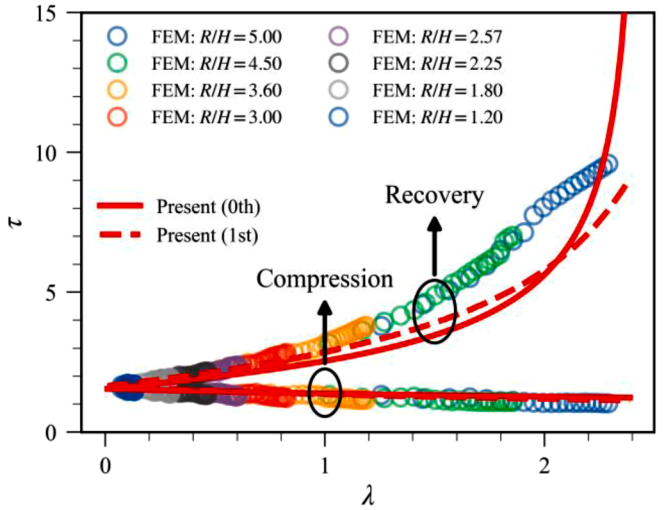

Fig. 8. Dimensionless compressive duration and recovery duration as functions of inelasticity parameter λ.

$$\tau_d = \tau_{\text{Hertz}} \exp\left(0.23\lambda^{1.80}\right) \tag{55}$$

shown by Fig. 7, or equivalently,

$$t_d = 2.865\left(\frac{m^*}{E^*}\right)^{\frac{2}{5}} R^{-\frac{1}{5}} V_0^{-\frac{1}{5}} \exp\left(0.23\lambda^{1.80}\right)$$

Because $\lambda^{1.8}$ emerges in the exponential function, given a certain thickness H, the contact duration is not necessarily monotone decreasing with increasing impact velocity, different from the relationship $t_{\text{Hertz}} \propto V_0^{-0.2}$ in Hertz's impact theory.

In order to study the contact force asymmetry, we divide the impact process to two stages: compression and recovery, and use the ratio of recovery to compression duration as an indicator for the asymmetry. It is not possible to obtain an explicit expression for the first-order solution. However, we can obtain the duration of compression based on the zeroth-order solution. Differentiating Eq. (35) to obtain the compressive velocity:

$$\dot{\bar{\delta}}_0(\tau) = -\frac{\beta}{\omega_0}\exp(-\beta\tau)\sin(\omega_0\tau) + \exp(-\beta\tau)\cos(\omega_0\tau) \tag{56}$$

the duration of compression, τ_{dc}, is determined by:

$$-\frac{\beta}{\omega_0}\exp(-\beta\tau_{dc})\sin(\omega_0\tau_{dc}) + \exp(-\beta\tau_{dc})\cos(\omega_0\tau_{dc}) = 0 \tag{57}$$

Simplifying Eq. (57), we have

$$\tau_{dc} = \frac{1}{\omega_0}\arctan\left(\frac{\omega_0}{\beta}\right) \tag{58}$$

Substituting Eqs. (32) and (33) to Eq. (58), we obtain the expression of τ_{dc} with respect to λ only:

$$\tau_{dc} = \frac{2\arctan\left(\sqrt{\frac{4}{\lambda^2}\left(\lambda + \left(\frac{5}{4}\right)^{-\frac{3}{5}}\right)^{\frac{1}{3}} - 1}\right)}{\sqrt{4\left(\lambda + \left(\frac{5}{4}\right)^{-\frac{3}{5}}\right)^{-\frac{1}{3}} - \left(\lambda + \left(\frac{5}{4}\right)^{-\frac{3}{5}}\right)^{-\frac{2}{3}}\lambda^2}} \tag{59}$$

Further, the duration of recovery, τ_{dr}, can be obtained by subtracting the duration of compression from the total contact duration:

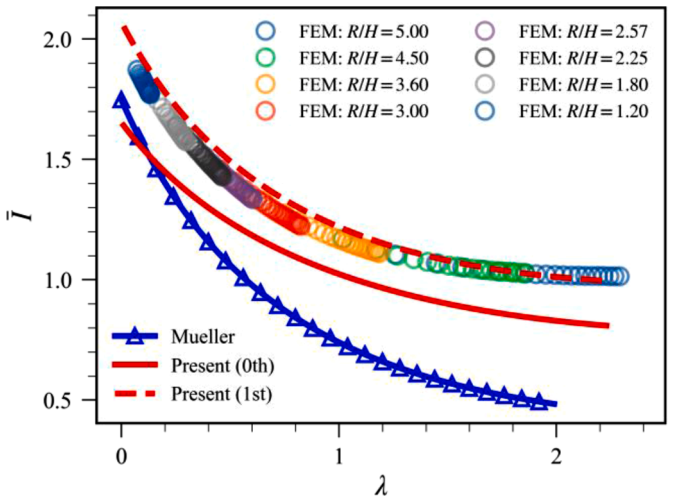

Fig. 9. Dimensionless impulse as function of inelasticity parameter λ.

$$\tau_{dr} = \tau_d - \tau_{dc} = \frac{2\pi - 2\arctan\left(\sqrt{\frac{4}{\lambda^2}\left(\lambda + \left(\frac{5}{4}\right)^{-\frac{3}{5}}\right)^{\frac{1}{3}} - 1}\right)}{\sqrt{4\left(\lambda + \left(\frac{5}{4}\right)^{-\frac{3}{5}}\right)^{-\frac{1}{3}} - \left(\lambda + \left(\frac{5}{4}\right)^{-\frac{3}{5}}\right)^{-\frac{2}{3}}\lambda^2}} \tag{60}$$

Particularly, for $\lambda = 0$, we have $\tau_{dc} = \tau_{dr} = \tau_d/2$.

The asymmetry of contact force history can be quantified by the ratio of the duration of recovery to the duration of compression. We introduce an index of asymmetry, η, defined by:

$$\eta = \frac{\tau_{dr}}{\tau_{dc}} = \frac{\pi}{\arctan\left(\sqrt{\frac{4}{\lambda^2}\left(\lambda + \left(\frac{5}{4}\right)^{-\frac{3}{5}}\right)^{\frac{1}{3}} - 1}\right)} - 1 \tag{61}$$

To determine η based on the present first-order solution, we can first differentiate Eq. (42) and then find the root using numerical procedures to obtain the duration for compression. Fig. 8 shows the durations of compression and recovery as functions of λ. Particularly, as $\lambda \to 0$, the durations of compression and recovery are identical, i.e., $\eta = 1$ (symmetrical profile). As λ increases, the duration of compression decreases whereas the duration of recovery increases, and hence η increases.

We check the effect of compliance on the impulse, which is a substantial quantity determining the motions of sphere and plate (Zener, 1941). As shown by Fig. 9, the value of impulse by our prediction Eq. (47) decreases as λ increases. This trend is compared with Mueller's solution, showing a relative error between 12.60% and 52.63%. On the other hand, the relative error of the present first-order solution is less than 3.95%.

In sum, the present solutions can accurately predict the contact force history of an elastic impact between a sphere and a plate. The discussion above can provide a theoretical interpretation for the symmetry breaking by the plate compliance: the plate compliance, as a dissipative term, shortens the compression and prolongs the recovery.

3.4. Motions of sphere and plate

In this section, we use the impulse to formulate the motions of sphere and plate. The motion of sphere is governed by

$$m_1 V(t) = m_1 V_0 - I(t) \tag{62}$$

Substituting Eq. (48) to Eq. (62), we have

$$m_1 V(\tau) = m_1 V_0 - m^* V_0 \bar{I}(\tau) \tag{63}$$

Because $m^* \approx m_1$, by introducing $\overline{V} = V/V_0$, the dimensionless form of the motion of sphere is obtained.

$$\overline{V}(\tau) = 1 - \bar{I}(\tau) \tag{64}$$

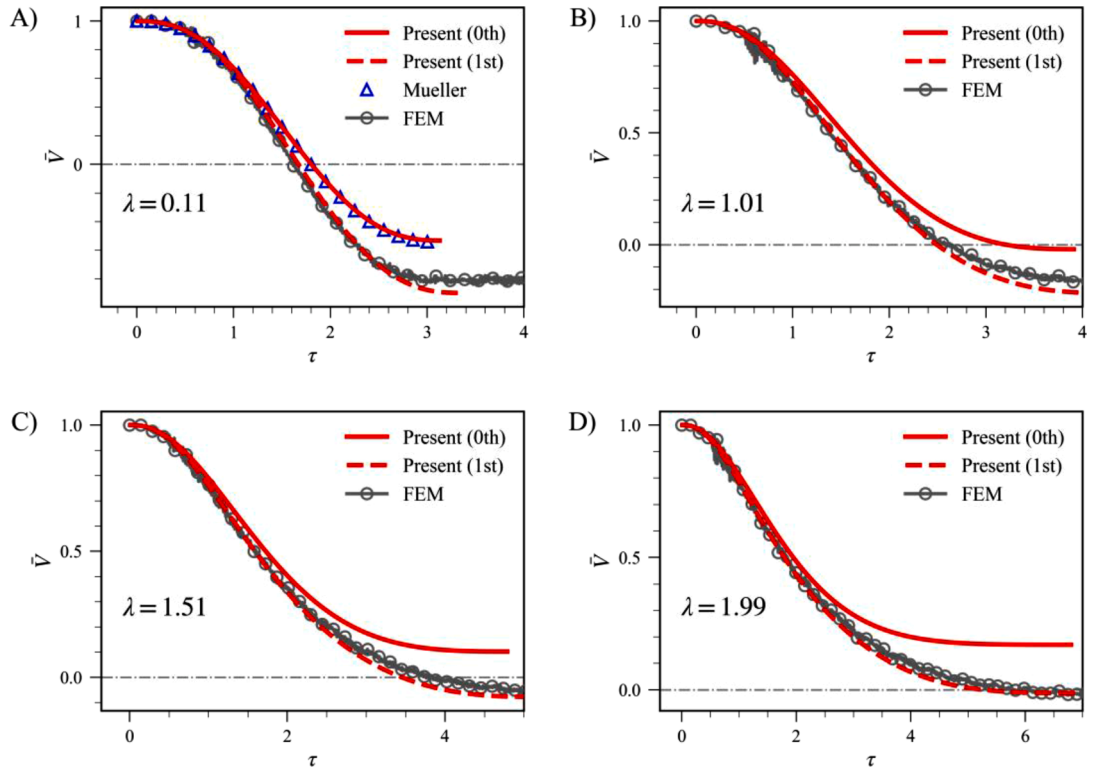

Fig. 10. History of dimensionless velocity of sphere for various inelasticity parameter λ: A) $\lambda = 0.11$, B) $\lambda = 1.01$, C) $\lambda = 1.51$, and D) $\lambda = 1.99$.

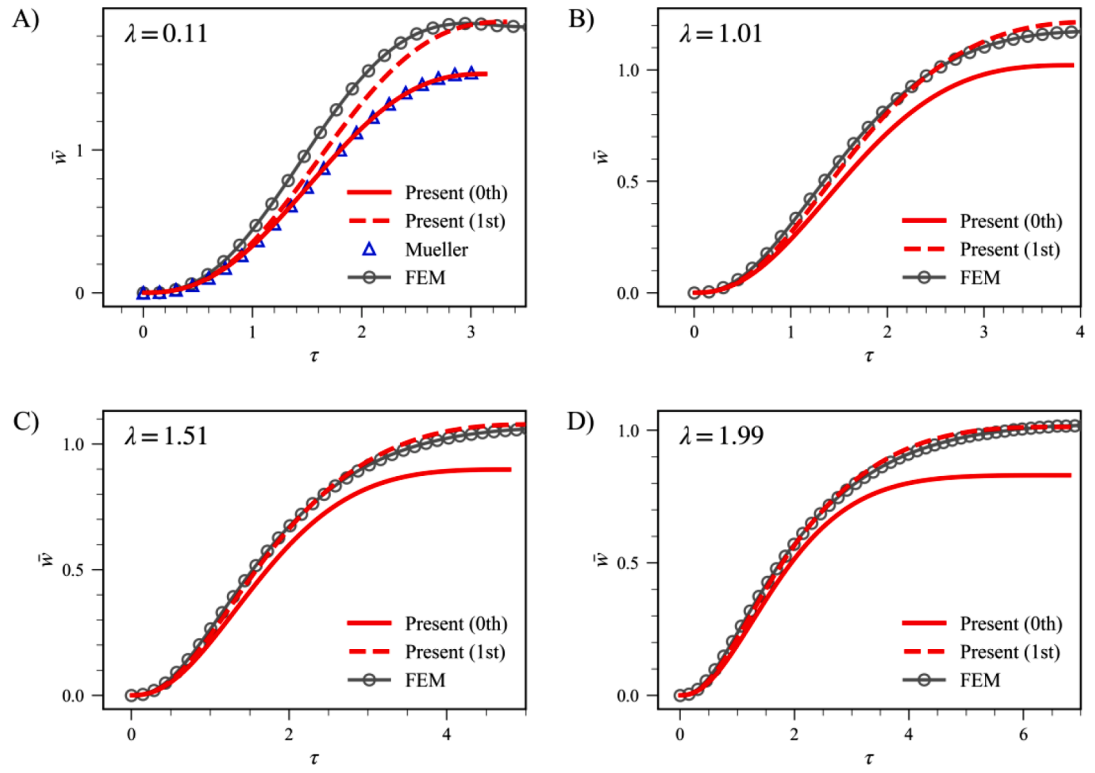

Fig. 11. History of dimensionless deflection of center of plate for various inelasticity parameter λ: A) $\lambda = 0.11$, B) $\lambda = 1.01$, C) $\lambda = 1.51$, and D) $\lambda = 1.99$.

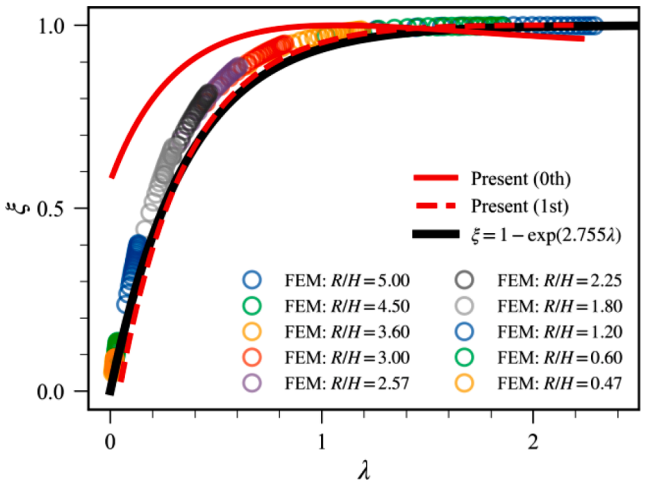

Fig. 12. Zener loss as function of inelasticity parameter λ.

Fig. 10 plots the histories of dimensionless velocity of the sphere for various λ. It is evident that the present first-order solution can predict very well the motion history of the sphere, for both small and large λ, while the present zeroth-order solution can only be used when λ is small.

To check the motion of sphere, we adopt Zener's formulation (Zener, 1941). Zener proposed a solution for the center deflection of the plate as follows.

$$w = \frac{1}{4\rho_2 H^2}\sqrt{\frac{3\rho_2(1-\nu_2^2)}{E_2}}I(t) \tag{65}$$

where w is the center deflection of the plate. Substituting Eq. (48) in Eq. (65), we can introduce the following dimensionless deflection for the plate:

$$\overline{w} = \frac{w}{\frac{m^* V_0}{4\rho_2 H^2}\sqrt{\frac{3\rho_2\left(1-\nu_2^2\right)}{E_2}}} = \overline{I}(\tau) \tag{66}$$

Fig. 11 shows the histories of dimensionless deflection of the center of the plate for various λ. Similar results can be found: the present first-order solution can best predict the motion of the plate, and the present zeroth-order solution will lead to large deviations when λ is large.

3.5. Semi-analytical model of the energy loss (Zener loss)

As in literature, one way for calculating energy loss is to use the terminal relative velocity $\dot{\bar{\delta}}(\tau_d)$. By this relative velocity, both the coefficient of restitution (Stronge, 1990) and the energy loss can be obtained. However, this approach is only valid for the case in which the velocity of plate center is much smaller than the velocity of the sphere, otherwise the energy loss of the sphere should be calculated by its own terminal velocity.

Instead of using the method above, we adopt the two other direct ways to calculate the energy loss for the Zener type impact: calculating kinetic energy loss using the motion of sphere, and integrating the work done using the contact force on the plate.

- As the first approach, because the velocity of the sphere evolves according to Eqs. (62) or (64), the loss of kinetic energy can be expressed by

$$W(t) = \frac{1}{2}m_1\left(V_0^2 - V^2(t)\right) \tag{67}$$

We can introduce the ratio of energy loss as follows

$$\xi = \frac{W}{\frac{1}{2}m_1 V_0^2} \tag{68}$$

With Eqs. (63), (64), (67) and (68), we have the following identity.

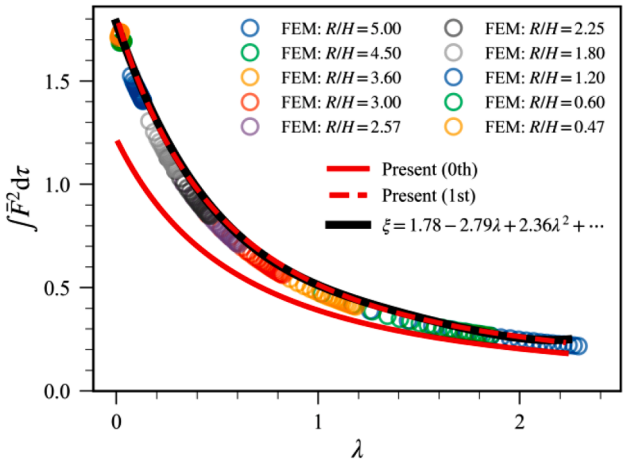

Fig. 13. Integration term in Eq. (76) as function of inelasticity parameter λ

$$\xi = 2\bar{I} - \bar{I}^2 \tag{69}$$

Mathematically, the energy loss ξ depends on the dissipative term $\lambda \frac{\mathrm{d}}{\mathrm{d}\tau}\bar{\delta}^3$; lager λ implies greater energy loss, as verified by both the present solutions and the FEM simulations in Fig. 12. Based on the present first-order solution, we can use the following semi-analytical approach to derive a simple identity for ξ. Given that $\xi \to 0$ as $\lambda \to 0$, and $\xi \to 1$ as $\lambda \to \infty$, we obtained the following expression for the Zener loss by fitting on the basis of the present first-order solution.

$$\xi = 1 - \exp(-2.755\lambda) \tag{70}$$

Comparison between Eq. (70) and the FEM results shows that the relative error of Eq. (70) is less than 10% for most of the cases and less than 1% for $\lambda \geq 1.61$.

Expanding Eq. (70), we find

$$\xi = 2.755\lambda - 3.795\lambda^2 + 3.485\lambda^3 - 2.400\lambda^4 + \ldots \tag{71}$$

For a small λ, we have approximately $\xi \approx 2.755\lambda$, and, in turn,

$$\xi \propto \left(\frac{R}{H}\right)^2 V_0^{0.2} \tag{72}$$

- As the second approach, the work done to the plate can be expressed as

$$W = \int F \mathrm{d}w \tag{73}$$

Substituting Eq. (65) to Eq. (73), we have

$$\begin{aligned} W &= \frac{1}{4\rho_2 H^2}\sqrt{\frac{3\rho_2\left(1-\nu_2^2\right)}{E_2}}\int F \mathrm{d}I \\ &= \frac{1}{4\rho_2 H^2}\sqrt{\frac{3\rho_2\left(1-\nu_2^2\right)}{E_2}}\int F^2 \mathrm{d}t \end{aligned} \tag{74}$$

Using dimensionless form of F and t, we have the expression for W:

$$W = \frac{1}{2}\chi m^* V_0^{\frac{11}{5}}\left(\frac{R}{H}\right)^2 \int \bar{F}^2 \mathrm{d}\tau \tag{75}$$

where χ is an introduced coefficient only depending on the material:

$$\chi = \frac{2\pi^{\frac{3}{5}}}{3^{\frac{1}{2}}}\sqrt{\frac{\rho_2(1-\nu_2^2)}{E_2}}\left(\frac{E^*}{\rho_2}\right)^{\frac{2}{5}}\left(\frac{\rho_1}{\rho_2}\right)^{\frac{3}{5}}$$

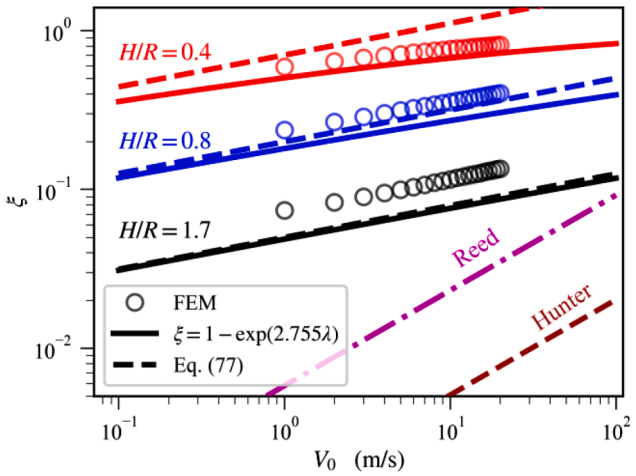

Fig. 14. Energy loss of sphere impacting plate as function of impact velocity

Hence, by $m^* \approx m_1$, we can obtain the ratio of energy loss as follows.

$$\xi = \frac{W}{\frac{1}{2}m_1 V_0^2} = \chi V_0^{\frac{1}{5}} \left(\frac{R}{H}\right)^2 \int_0^{\tau_d} \overline{F}^2 \mathrm{d}\tau \tag{76}$$

The integrand in Eq. (76) is only depending on λ, shown in Fig. 13. Further, we can use a representative polynomial function to replace $\int_0^{\tau_d} \overline{F}^2 \mathrm{d}\tau$ in the shown domain, i.e.

$$\int_0^{\tau_d} \overline{F}^2 \mathrm{d}\tau \approx 1.78 - 2.79\lambda + 2.36\lambda^2 + \ldots$$

so that

$$\xi \approx \chi V_0^{\frac{1}{5}} \left(\frac{R_1}{H}\right)^2 \left(1.78 - 2.79\lambda + 2.36\lambda^2 + \ldots\right)$$

For a small λ, we have

$$\xi \approx 1.78 \chi V_0^{\frac{1}{5}} \left(\frac{R}{H}\right)^2 \tag{77}$$

which shows an identical relationship with Eq. (72)

With Eqs. (70) and (77), we can plot the relationship of the energy loss with the impact velocity, shown by Fig. 14. First of all, the present semi-analytical model Eq. (70) shows good agreement with the FEM simulation. Second, for small λ, we find that the Zener loss is proportional to $V_0^{0.2}$, different from what Hunter and Reed suggested ($\xi \propto V_0^{0.6}$ for a sphere impacting on a half-space). Using the material properties in the present FEM simulation, we calculated Hunter's coefficient is $k_{\text{Hunter}} \approx 0.0013$ and Reed's coefficient is $k_{\text{Reed}} \approx 0.0058$, shown by Fig. 14. Obviously, their suggested relation $\xi \propto V_0^{0.6}$ cannot apply to the sphere-plate impact. The reason traces back to that Hunter formulated the symmetrical contact force history on the basis of uncoupled equation, which is substantially different from the case of Zener type impact. Third, we can use Eq. (77) for the cases with a thick plate such as $H = 1.7R$ under a wide range of impact velocity, and the cases with a thin plate under a small impact velocity which, for example, is less than 0.5 m/s for the case with $H = 0.4R$.

From the view of energy dissipation, the energy loss of Hunter type and Reed type are the result of stress wave traveling in the half-space. When a sphere impacts a large plate, compared with the Hunter loss or Reed loss, the flexural wave might take a large fraction of energy dissipation. In the Zener equation, mathematically, the energy loss originates from the dissipative term $\lambda \frac{\mathrm{d}}{\mathrm{d}\tau}\overline{\delta}^{\frac{3}{2}}$, leading to that the energy dissipation by flexural wave is a function of λ. While λ is proportional to $V_0^{0.2}$ by definition, the energy loss ξ is also proportional to $V_0^{0.2}$ when λ is small.

In sum, on one hand, for a small energy loss, we can use the relationship Eq. (77) for simplicity to estimate the energy loss of a sphere impacting on a plate. Different from the relationship $\xi \propto V_0^{0.6}$ suggested by Hunter and Reed for the case of a sphere impacting on a half-space, the ratio of energy loss of Zener type is proportional to $V_0^{0.2}$. On the other hand, for a large energy dissipation, we can use

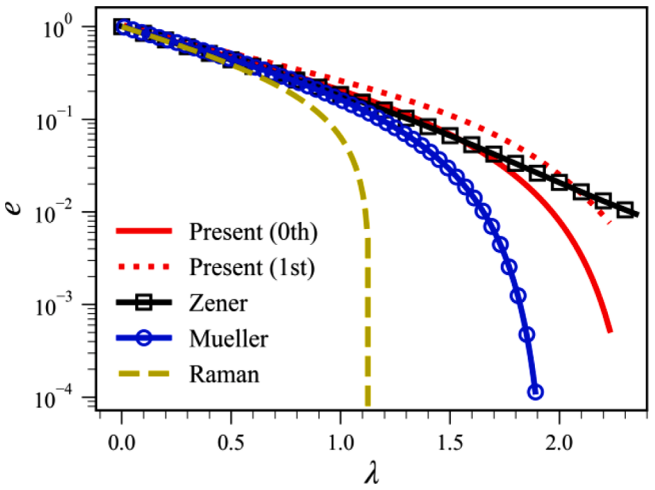

Fig. 15. Coefficient of restitution as function of inelasticity parameter λ.

Eq. (70) to predict the energy loss of Zener type.

3.6. Coefficient of restitution

Based on Zener's equation, the coefficient of restitution, e, is defined by the terminal relative velocity, $\dot{\bar{\delta}}(\tau_d)$, which is different from the residual velocity of the sphere. For the zeroth-order solution, the sphere detaches from the plate at time $\tau_d = 2\pi / \sqrt{4k - k^2\lambda^2}$, so we have

$$\frac{\mathrm{d}\bar{\delta}}{\mathrm{d}\tau} = \exp\left(-\frac{k\lambda}{2}\tau\right) \tag{78}$$

and the coefficient of restitution can be expressed by

$$e = \exp\left(-\frac{\pi\lambda}{\sqrt{4k^{-1} - \lambda^2}}\right) \tag{79}$$

Substituting Eq. (25) into Eq. (79), we obtain expression for e with respect to the inelasticity parameter λ only:

$$e = \exp\left(-\frac{\pi\lambda}{\sqrt{4\left(\lambda + \left(\frac{5}{4}\right)^{-\frac{3}{5}}\right)^{\frac{1}{3}} - \lambda^2}}\right) \tag{80}$$

The validity of Eq. (80) locates in the region of $\lambda \le 2/\sqrt{k}$, namely

$$4\left(\lambda + \left(\frac{5}{4}\right)^{-\frac{3}{5}}\right)^{\frac{1}{3}} > \lambda^2 \tag{81}$$

Simplifying Inequation (81) reveals that Eq. (80) can be used for $\lambda \in [0,\ 2.442)$. Compared with the restriction that $\lambda < 2$ suggested by Mueller's solution (Mueller et al., 2015), Eq. (80) imposes a weaker restriction.

In the sense of the coefficient of restitution defined by terminal relative velocity, we also numerically computed e by substituting τ_d into the derivative of Eq. (42), shown by Fig. 15. For comparison, we also plots Raman's model (Raman, 1920; Zener, 1941) and the numerically integrated results with Zener's equation (Zener, 1941). On one hand, Raman's model is valid only for very small λ ($\lambda < 0.4$), Mueller's model extended the range to $\lambda \le 0.85$, while the present model Eq. (80) derived from the zeroth-order solution extends the applicable region to $\lambda \le 1.8$. On the other hand, the present first-order solution can predict the coefficient of restitution for a large range of λ, but for $1.0 \le \lambda \le 1.8$, the prediction is not better than that of the present zeroth-order solution. Considering both engineering conveniency and accuracy, we suggest that Eq. (80) may be the preferred model for the estimation of the coefficient of restitution for the elastic impact of a sphere on a plate.

4. Conclusion

Using homotopy analysis method, we proposed an analytical solution to Zener's equation to predict the elastic impact between a sphere and a large plate. Using the obtained contact force history, we studied the energy loss due to the flexural wave, as well as the motion of the sphere and plate during the impact. The conclusions are as follows:

1 By solving Zener's equation, we obtained the contact force history up to the first order of the homotopy embedding parameter (Eqs. (35) and (42)). These analytical solutions provided a theoretical foundation for understanding the elongation of contact duration by structural compliance and in turn the break of contact force symmetry.
2 Energy loss of Zener type can be predicted by the present first-order solution accurately; also, we provided a semi-analytical model (Eq. 70) for this type of energy loss. For small plate compliance, Eq. (77) can be used to determine Zener loss for simplicity, revealing that the energy loss is proportional to $V_0^{0.2}$, which is different from the energy loss relationship ($\xi \propto V_0^{0.6}$) suggested by Hunter and Reed.
3 The present first-order solution can accurately predict the motion of sphere, the deflection of the plate, and energy loss by flexural wave. With the present zeroth-order solution, we also obtained an explicit expression Eq. (80) for the coefficient of restitution, which can predict well in the range of $\lambda \leq 1.8$.

Declaration of Competing Interest

The authors declare that they have no known competing financial interests or personal relationships that could have appeared to influence the work reported in this paper.

Acknowledgment

This work was supported by the National Natural Science Foundation of China (No. 11772334, 11890681, 12022210, 12032001), by the Youth Innovation Promotion Association CAS (2018022), by the Strategic Priority Research Program of the Chinese Academy of Sciences (No. XDB22040501). We would like to acknowledge anonymous reviewers and Prof. X.H. Shi for their helpful comments and discussions.

Appendix: FEM simulation

FEM simulations were conducted using ABAQUS commercial software (Dassualt Systèmes, Vélizy-Villacoublay, France) with an explicit solver. Due to the symmetry, only an axisymmetric model was necessary, shown in Fig. 16. The radius of the sphere R was set to 0.9 mm. The radius of the plate was set to 150 mm, sufficiently large to eliminate boundary effects (possible wave reflection). A contact pair was established between the sphere and the plate: the penalty method of constraint enforcement was applied on the normal direction for the pressure-overclosure relationship ('Hard' contact in ABAQUS), and the friction coefficient was set to 0.1. The materials for the elastic sphere and the elastic plate are γAl_2O_3 and glass, respectively. Detailed material parameters are listed in Table 1. After a mesh dependency check, the element (CAX4R) count in this model was about 23,000, with the finest element size at the contact region being 1%R. To study the compliance of plate on the impact process, we set the impact speed ranging from 1 m/s to 20 m/s and the thickness of plate ranging from 0.18 mm to 0.75 mm to enable a wide range of λ.

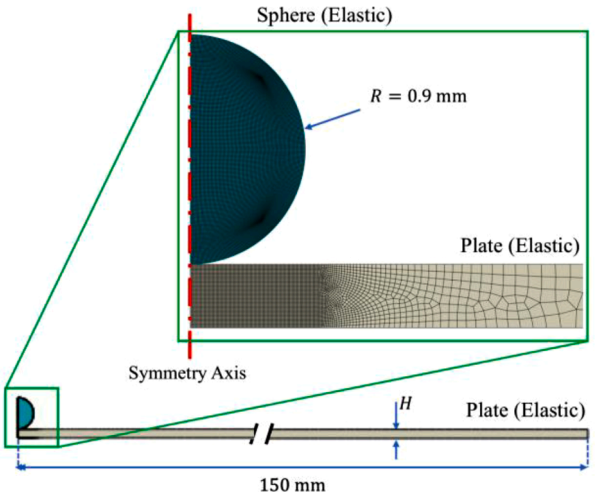

Fig. 16. FEM model for an elastoplastic sphere impacting an elastic plate.

Table 1
Material properties for FEM model.

	Sphere	Plate
Material	γAl_2O_3	glass
Young's Modules (GPa)	12.23	73
Poisson Ratio	0.21	0.21
Density (kg/m^3)	879	2500

References

Abbasbandy, S., 2006. The application of homotopy analysis method to nonlinear equations arising in heat transfer. Phys. Lett. A 360, 109–113.
Abbasbandy, S., 2007. The application of homotopy analysis method to solve a generalized Hirota-Satsuma coupled KdV equation. Phys. Lett. A 361, 478–483.
Abbasbandy, S., 2008. Solitary wave solutions to the Kuramoto-Sivashinsky equation by means of the homotopy analysis method. Nonlinear Dyn. 52, 35–40.
Aboudi, J., 1978. Dynamic contact stresses caused by impact of a non-linear elastic half-space by an axisymmetrical projectile. Comput. Methods Appl. Mech. Eng. 13, 189–204.
Arfken, G.B., Weber, H.J., Harris, F.E., 2013. Mathematical Methods for Physicists: a Comprehensive Guide, 7th ed. Elsevier, Amsterdam; Boston.
Boettcher, R., Kunik, M., Eichmann, S., Russell, A., Mueller, P., 2017a. Revisiting energy dissipation due to elastic waves at impact of spheres on large thick plates. Int. J. Impact Eng. 104, 45–54.
Boettcher, R., Russell, A., Mueller, P., 2017b. Energy dissipation during impacts of spheres on plates: Investigation of developing elastic flexural waves. Int. J. Solids Struct. 106, 229–239.
Ciavarella, M., Joe, J., Papangelo, A., Barber, J.R., 2019. The role of adhesion in contact mechanics. J. R. Soc. Interface 16, 22.
Dormand, J.R., Prince, P.J., 1980. A family of embedded Runge-Kutta formulae. J. Comput. Appl. Math. 6, 19–26.
Feng, X.Q., Li, H., Zhao, H.P., Yu, S.W., 2009. Numerical simulations of the normal impact of adhesive microparticles with a rigid substrate. Powder Technol. 189, 34–41.
Flores, P., Machado, M., Silva, M.T., Martins, J.M., 2011. On the continuous contact force models for soft materials in multibody dynamics. Multibody Syst. Dyn. 25, 357–375.
Hertz, H., 1882. Ueber die Berührung fester elastischer Körper. J. für die reine und Angew. Math. Crelles J. 1882, 156–171.
Hille, E., 1968. Lectures on Ordinary Differential Equations. Addison-Wesley Pub. Co., New York.
Hunter, S.C., 1957. Energy absorbed by elastic waves during impact. J. Mech. Phys. Solids 5, 162–171.
Hunter, S.C., 1960. The Hertz problem for a rigid spherical indenter and a viscoelastic half-space. J. Mech. Phys. Solids 8, 219–234.
Hutchings, I.M., 1979. Energy absorbed by elastic-waves during plastic impact. J. Phys. D Appl. Phys. 12, 1819–1824.
Johnson, K.L., 1985. Contact Mechanics. Cambridge University Press, Cambridge Cambridgeshire; New York.
Koller, M.G., Kolsky, H., 1987. Waves produced by the elastic impact of spheres on thick plates. Int. J. Solids Struct. 23, 1387–1400.
Landau, L.D., Lifshits, E.M., Kosevich, A.M., Pitaevskii, L.P., 1986. Theory of Elasticity, 3rd English ed. Pergamon Press, Oxford Oxfordshire; New York.
Lankarani, H.M., Nikravesh, P.E., 1990. A contact force model with hysteresis damping for impact analysis of multibody systems. J. Mech. Des. 112, 369–376.
Lee, E.H., 1940. The impact of a mass striking a beam. J. Appl. Mech. 7, A129–A138.
Liao, S., 2012. Homotopy Analysis Method in Nonlinear Differential Equations. Springer, Heidelberg; New York.
Liao, S., 2014. Advances in the Homotopy Analysis Method. World Scientific, Hackensack New Jersey.
Lifshitz, J.M., Kolsky, H., 1964. Some experiments on an elastic rebound. J. Mech. Phys. Solids 12, 35–43.
Love, A.E.H., 1944. A Treatise on the Mathematical Theory of Elasticity, 4th ed. Dover Publications, New York.
Maier, L.R., Tsai, Y.M., 1974. Wave-propagation in linear viscoelastic plates of various thicknesses. J. Mech. Phys. Solids 22, 1–16.
Mueller, P., Boettcher, R., Russell, A., Truee, M., Tomas, J., 2015. A novel approach to evaluate the elastic impact of spheres on thin plates. Chem. Eng. Sci. 138, 689–697.
Muller, P., Bottcher, R., Russell, A., True, M., Aman, S., Tomas, J., 2016. Contact time at impact of spheres on large thin plates. Adv. Powder Technol. 27, 1233–1243.
Nayfeh, A.H., 2000. Perturbation Methods. John Wiley & Sons, New York.
Patil, D., Higgs, C.F., 2017. A coefficient of restitution model for sphere-plate elastoplastic impact with flexural vibrations. Nonlinear Dyn. 88, 1817–1832.
Peng, B., Feng, X.Q., Li, Q.Y., 2020. Decohesion of a rigid flat punch from an elastic layer of finite thickness. J. Mech. Phys. Solids 139, 103937.
Peng, Q., Jin, Y., Liu, X., Wei, Y.G., 2021. Effect of plasticity on the coefficient of restitution of an elastoplastic sphere impacting an elastic plate. Int. J. Solids Struct. 222–223.
Raman, C.V., 1920. On some applications of Hertz's theory of impact. Phys. Rev. 15, 277–284.
Reed, J., 1985. Energy-losses due to elastic wave-propagation during an elastic impact. J. Phys. D Appl. Phys. 18, 2329–2337.
Shampine, L.F., 1986. Some practical Runge-Kutta formulas. Math. Comput. 46, 135–150.
Stronge, W.J., 1990. Rigid body collisions with friction. Proc. R. Soc. Lond. Ser. A Math. Phys. Eng. Sci. 431, 169–181.
Stronge, W.J., 2000. Contact problems for elasto-plastic impact in multi-body systems. Impacts Mech. Syst. Anal. Model. 551, 189–234.
Stronge, W.J., 2019. Impact Mechanics, 2nd ed. University of Cambridge, Cambridge, United Kingdom; New York, USA.
Thornton, C., 1997. Coefficient of restitution for collinear collisions of elastic perfectly plastic spheres. J. Appl. Mech. Trans. ASME 64, 383–386.
Thornton, C., Cummins, S.J., Cleary, P.W., 2017. On elastic-plastic normal contact force models, with and without adhesion. Powder Technol. 315, 339–346.
Tillett, J.P.A., 1954. A study of the impact on spheres of plates. Proc. Phys. Soc. Lond. Sect. B 67, 677–688.
Wu, C.Y., Li, L.Y., Thornton, C., 2003. Rebound behavior of spheres for plastic impacts. Int. J. Impact Eng. 28, 929–946.
Wu, C.Y., Li, L.Y., Thornton, C., 2005. Energy dissipation during normal impact of elastic and elastic-plastic spheres. Int. J. Impact Eng. 32, 593–604.
Yabushita, K., Yamashita, M., Tsuboi, K., 2007. An analytic solution of projectile motion with the quadratic resistance law using the homotopy analysis method. J. Phys. A Math. Theor. 40, 8403–8416.
Zener, C., 1941. The intrinsic inelasticity of large plates. Phys. Rev. 59, 669–673.